ELSEVIER

Spectrochimica Acta Part B 61 (2006) 623 – 633

SPECTROCHIMICA ACTA PART B

www.elsevier.com/locate/sab

Experimental evaluation of the cross-sections for the $Cs(6D) \rightarrow Cs(7P_J)$ and $Cs(6D_{5/2}) \rightarrow Cs(6D_{3/2})$ collisional transfer processes induced by He and Ar☆

Tiffany L. Correll [a], Vlasta Horvatic [b,*], Nicoló Omenetto [a], James D. Winefordner [a], Cedomil Vadla [b]

[a] *Department of Chemistry, University of Florida, Gainesville, FL 32611, USA*
[b] *Institute of Physics, 10000 Zagreb, Croatia*

Received 14 June 2005; accepted 2 August 2005
Available online 9 September 2005

Abstract

The cross-sections for collisional excitation transfer $Cs(6D) \overset{Q_{D3}}{\rightarrow} Cs(7P_{1/2})$ and $Cs(6D) \overset{Q_{D4}}{\rightarrow} Cs(7P_{3/2})$, and fine structure mixing $Cs(6D_{5/2}) \overset{Q_{65}}{\rightarrow} Cs(6D_{3/2})$ due to collisions with helium and argon atoms at temperatures in the range between 333 and 367 K were determined using atomic fluorescence. The cross-sections for the processes $Cs(6D)+He, Ar \rightarrow Cs(7P_J)+He, Ar$ were found to be $Q_{D3}^{He}=(0.9\pm0.4)\times10^{-16}$ cm^2, $Q_{D4}^{He}=(2.6\pm1.2)\times10^{-16}$ cm^2, $Q_{D3}^{Ar}=(1.2\pm0.6)\times10^{-18}$ cm^2 and $Q_{D4}^{Ar}=(2.6\pm1.3)\times10^{-18}$ cm^2. These values are consistent with the results obtained at higher temperatures and reported previously. The cross-sections for the He and Ar-induced $6D_J$ fine-structure mixing were determined to be $Q_{65}^{He}=(54\pm15)\times10^{-16}$ cm^2 and $Q_{65}^{Ar}=(17\pm5)\times10^{-16}$ cm^2 and were found to fit very well into the existing body of cross-section data for intra-multiplet ($nP_{1/2} \rightarrow nP_{3/2}$; $nD_{5/2} \rightarrow nD_{3/2}$) mixing in cesium induced by collisions with helium and argon.

Keywords: Cross-sections; Energy transfer; Collision transfer; Cesium; Alkali-noble gas mixture

1. Introduction

Collisional excitation energy transfer (CEET) occurring as a result of thermal collisions between excited atoms and molecules in gases has been extensively studied during the last decades. The cross-sections for CEET processes occurring in excited pure or mixed alkali vapors constitute the vast majority of the body of the CEET cross-sections data published so far. Krause [1] has summarized in a review paper the most relevant experimental and theoretical results available in this area until 1975. In addition, an extensive list of more recent references pertaining to this subject can be found in Refs. [2–4]. Alkalis owe their popularity to the relative simplicity they offer to experimental and theoretical treatment. Nevertheless, the discrepancies between theoretical and experimental results, as well as among experimental results reported by different authors for the same CEET process are frequent, so that several measurements published by different groups of authors are usually taken into account in establishing reliable values for the cross-section of a given process.

CEET processes are important mechanisms for establishing the population distributions, and very often play a crucial role in many phenomena in excited gaseous media. Studies of such interactions are of great interest in a variety of fields, of both fundamental and applied nature. One aim of the present investigation, oriented towards applicative purposes, is to quantitatively characterize the system in view of developing cesium based atomic line filters and imaging detectors [5–10]. The other one is contribute to the existing database of the

☆ This article is published in a special honor issue of Spectrochimica Acta Part B dedicated to the memory of Prof. Howard V. Malmstadt, in recognition of his many outstanding contributions to spectrochemical analysis, in areas of research, leadership, and teaching.

* Corresponding author. Tel.: +385 1 469 8861; fax: +385 1 469 8889.
E-mail address: blecic@ifs.hr (V. Horvatic).

0584-8547/$ - see front matter © 2005 Elsevier B.V. All rights reserved.
doi:10.1016/j.sab.2005.08.002

cross-sections for exothermic CEET processes in alkali vapors by adding the values of two reactions in cesium induced by collisions with helium and argon atoms.

The purpose of this paper is to report and discuss the experimental evaluation of the inter-multiplet collisional transfer processes

$$\mathrm{Cs(6D)} + \mathrm{He(or\ Ar)} \overset{Q_{D3}}{\rightarrow} \mathrm{Cs}\left(7\mathrm{P}_{1/2}\right) + \mathrm{He(or\ Ar)}$$

$$\mathrm{Cs(6D)} + \mathrm{He(or\ Ar)} \overset{Q_{D4}}{\rightarrow} \mathrm{Cs}\left(7\mathrm{P}_{3/2}\right) + \mathrm{He(or\ Ar)} \qquad (1)$$

and of the intra-multiplet (fine-structure) mixing process

$$\mathrm{Cs}\left(6\mathrm{D}_{5/2}\right) + \mathrm{He(or\ Ar)} \overset{Q_{65}}{\rightarrow} \mathrm{Cs}\left(6\mathrm{D}_{3/2}\right) + \mathrm{He(or\ Ar)} \qquad (2)$$

The above reactions have been investigated in the temperature range between 333 and 367 K.

The processes in Eq. (1) were investigated previously by Cuvellier et al. [11]. They reported J-selective cross-sections values for the endothermic processes $\mathrm{Cs}(7\mathrm{P}_J) \rightarrow \mathrm{Cs}(6\mathrm{D}_{3/2})$ at temperatures of 450 and 615 K, with He and Ar as perturbers. The cross-sections for the corresponding exothermic reactions, obtained by applying the principle of the detailed balancing to the results of [11], are in good agreement with the cross-sections obtained here for the processes in Eq. (1) at lower temperatures.

To our knowledge, the cross-sections for neither exothermic nor endothermic $\mathrm{Cs}(6\mathrm{D}_J)$ fine structure mixing induced by collisions with helium and argon atoms have been investigated so far. The cross-sections Q_{65}^{He} and Q_{65}^{Ar} for the reaction (2) are reported here for the first time.

2. Experiment

2.1. Experimental details

Helium and argon-induced $\mathrm{Cs(6D)} \rightarrow \mathrm{Cs}(7\mathrm{P}_J)$ and $\mathrm{Cs}(6\mathrm{D}_{5/2}) \rightarrow \mathrm{Cs}(6\mathrm{D}_{3/2})$ collisional mixing was investigated with the experimental arrangement previously described in detail in Ref. [12]. For the readers' convenience, the important details are repeated here. The schematic experimental set-up is shown in the inset of Fig. 1. Cesium vapors were created in a resistively heated, cross-shaped stainless-steal heat-pipe oven with quartz windows, which was not operated in the heat-pipe mode. Helium or argon was used as a buffer gas. The total pressure in the heat pipe was measured with a MKS Baratron manometer. The length of the vapor column was $L = (6 \pm 1)$ cm.

Cesium atoms were excited to $6\mathrm{D}_{5/2}$ state by two counter-propagating lasers following the two-step $6\mathrm{S}_{1/2} \rightarrow 6\mathrm{P}_{3/2} \rightarrow 6\mathrm{D}_{5/2}$ excitation scheme. In the first excitation step, a single-mode laser diode DL1 (Qphotonics, model QLD-850-100S, $\lambda = 850$ nm at 25 °C, maximum power 100 mW) was used to excite the red wing of the $6\mathrm{S}_{1/2}(F=4) \rightarrow 6\mathrm{P}_{3/2}(F=3,4,5)$ hyperfine transition. The second step excitation was performed with a single-mode laser diode DL2 (Qphotonics, model QLD-820-100S, $\lambda = 918$ nm at 25 °C, maximum power 100 mW) centered on $6\mathrm{P}_{3/2} \rightarrow 6\mathrm{D}_{5/2}$ transition. Current and temperature control of the laser diodes were provided by commercial diode laser drivers (PROFILE Optische Systeme GmbH, model ITC 502).

Both laser beams were collimated and characterized by a bell-shaped power distribution across the beam. The central part of the collimated laser beams (diameter: 2 mm), having

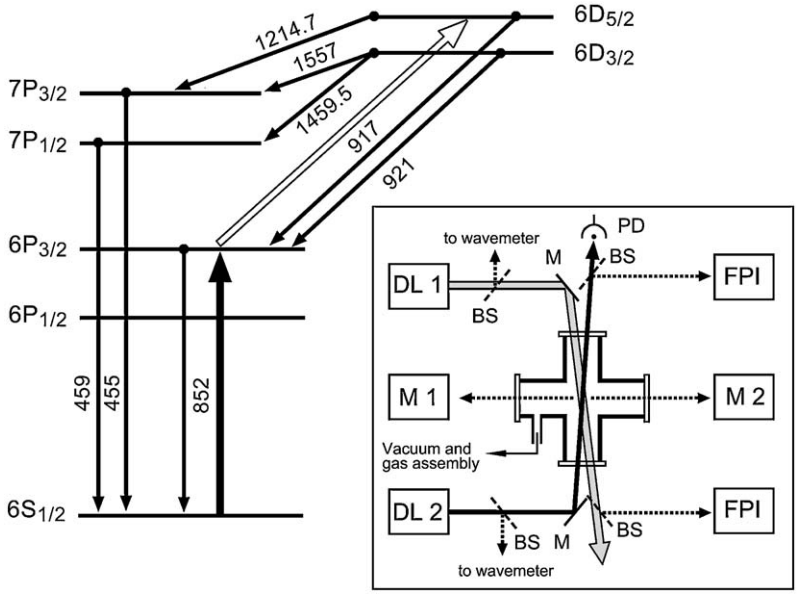

Fig. 1. Partial energy level diagram of cesium depicting the laser pumped (852 and 917 nm) and radiative transitions among the indicated levels. The collisional mixing rates are not shown. The numbers represent the wavelengths (in nm) of the transitions. The inset shows the experimental setup used to conduct He and Ar-induced CEET studies in cesium. M1, M2 = monochromators, DL1, DL2 = laser diodes, BS = beam splitter, FPI = Fabry–Perot interferometer, M = mirror and PD = photodiode. The inclination of the laser beams inside the heat pipe is exaggerated.

a nearly homogeneous power distribution, was used for the excitation. The typical laser powers of the 852 and 917 nm radiation, measured just in front of the heat-pipe entrance windows, were 19 and 9 mW, respectively. The laser power was measured with a power meter (Coherent, model Filedmaster LM-2). Each beam was split into three parts. One part was directed to a confocal, 2 GHz free spectral range, scanning Fabry–Perot interferometer (FPI), which was used to monitor the single-mode operation and the frequency stability of the laser diodes, as well as for calibration of the absorption spectra (in the non-scanning FPI mode).

The second part of the beam was used for wavelength calibration by a commercial wavemeter (Burleigh Instruments Inc, model WA-20VIS). The major part of each beam was directed through the heat pipe oven containing cesium, and the fluorescence was monitored through the heat pipe side arms at right angles to the laser beams' propagation direction.

The fluorescence intensities of the spontaneous emission at $6D_{3/2,\ 5/2} \rightarrow 6P_{3/2}$ (921 and 917 nm lines) and $7P_{1/2,\ 3/2} \rightarrow 6S_{1/2}$ (459 and 455 nm lines) transitions were analyzed by two monochromators. The central part (length: ≈1 cm) of the cylindrical fluorescence zone was imaged onto the entrance slits of the monochromators (M1 and M2 in Fig. 1). A 0.5 m monochromator (M1, Jarrell–Ash, model 82025) equipped with a Peltier-cooled photomultiplier (model RCA 7102, S1 cathode) was used to measure the 917 and 921 nm fluorescence. The blue fluorescence at 455 and 459 nm was measured with a 1 m monochromator (M2, McPherson, model 2051) supplied with an S11 cathode photomultiplier (model EMI 9524S). On one side of the heat pipe arm the fluorescence was collected with mirrors (periscope arrangement) and focused onto the entrance slit of the Jarrell–Ash monochromator (M1). On the opposite side, the fluorescence was collected by means of a slit-type fiber optic bundle and imaged onto the entrance slit of the McPherson (M2) monochromator.

The calibration between the two detection systems was established by measuring simultaneously the 455 and 459 nm intensities with both the McPherson/PMT arrangement and the Jarrell Ash/PMT assembly. This was possible at He pressures of ~10 mbar, since in this case the blue fluorescence signals were large enough to be detected also with the Jarrell Ash/PMT system. By comparison of these simultaneously measured blue fluorescence signals, a calibration factor connecting the two detection systems could therefore be determined. At all other noble gas pressures in the investigated range, the 455 and 459 nm intensities measured with McPherson/PMT system were converted in terms of the Jarrell Ash/PMT response, using the calibration factor thus obtained. Also, all signals were corrected for the responsivity of optical transmission and detection of the Jarrell Ash/PTM system which was measured with a calibrated tungsten-ribbon lamp (PHILIPS model W2KGV22i).

In order to evaluate the cesium ground-state number density, an unsaturated ground state absorption measurement was performed. The 852 nm diode laser was scanned across the $6S_{1/2} \rightarrow 6P_{3/2}$ transition by tuning the temperature of the laser, its power being reduced down to ~10 μW by means of neutral density filters. The transmitted radiation was detected by a photodiode and the confocal FPI was used to calibrate the dispersion of the spectrum. The cesium ground-state number densities in the present experiment varied between 1×10^{12} cm^{-3} and 1×10^{13} cm^{-3}. The corresponding temperatures of the cesium vapor, subsequently obtained using published values for the vapor pressure curve of cesium [13,14], were in the range between 333 an 367 K.

2.2. Determination of the cross-sections

One of the essential steps in the procedure of the determination of the cross-sections is to define an

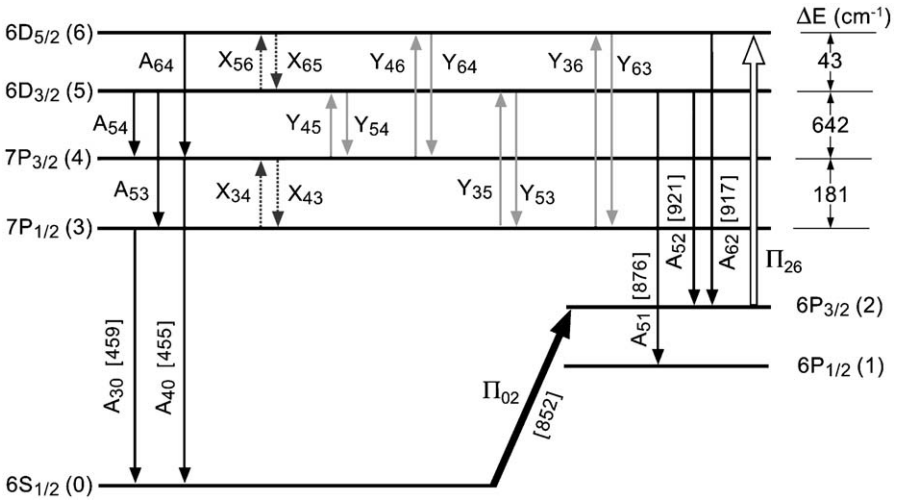

Fig. 2. Partial energy level diagram of cesium depicting the states relevant for the determination of the cross-sections investigated in the present experiment (see text). The energy separations, ΔE, between the $6D_{3/2}$ and $7P_{3/2}$ states as well as the fine structure splitting of the $6D_J$ and $7P_J$ states are also indicated.

adequate set of rate equations pertinent to the processes of interest. A detailed term diagram involving the states relevant for the determination of the cross-sections investigated here is shown in Fig. 2. The levels $6S_{1/2}$, $6P_{1/2}$, $6P_{3/2}$, $7P_{1/2}$, $7P_{3/2}$, $6D_{3/2}$ and $6D_{5/2}$ are denoted with numbers 0 to 6, respectively. The spontaneous emission rates are labeled with As, while Xs and Ys denote intra-multiplet and inter-multiplet mixing rates due to Cs and noble gas-induced collisional transfer, respectively. The numbers in square brackets represent the (rounded off) wavelengths of the respective transitions. The pump rates of the laser excited transitions in the first and the second step are labeled with Π_{02} and Π_{26}. In principle, one should consider that, in addition to the processes indicated, states 3–6 can also be populated by the energy pooling processes $Cs^*(6P_{3/2})+Cs^*(6P_{3/2})\rightarrow Cs^{**}(n)+Cs(6S_{1/2})$ ($n=3$–6 and higher lying states not shown here) and subsequent collisional mixing and radiative relaxation of the highly excited $Cs^{**}(n)$ states. However, calculations using the available cross-sections for the energy pooling in cesium [15,16] show that these contributions can safely be neglected under the conditions of the present experiment.

Therefore, the set of the rate equations corresponding to the scheme given in Fig. 2 can be represented in the following matrix form:

$$\begin{pmatrix} -(1/\tau_3+X_{34}+Y_{35}+Y_{36}) & X_{43} & (A_{53}+Y_{53}) & Y_{63} \\ X_{34} & -(1/\tau_4+X_{43}+Y_{45}+Y_{46}) & (A_{54}+Y_{54}) & (A_{64}+Y_{64}) \\ Y_{35} & Y_{45} & -(1/\tau_5+Y_{53}+Y_{54}+X_{56}) & X_{65} \\ Y_{36} & Y_{46} & X_{56} & -(1/\tau_6+Y_{63}+Y_{64}+X_{65}) \end{pmatrix} \times \begin{pmatrix} N_3 \\ N_4 \\ N_5 \\ N_6 \end{pmatrix} = \begin{pmatrix} 0 \\ 0 \\ 0 \\ -\Pi_{26} \end{pmatrix}. \tag{3}$$

By taking into account the values of the cross-sections for the inter-multiplet mixing (Q_{i5}, Q_{i6}, $i=3$, 4, see Table 1) it turns out that in Eq. (3), under the present experimental conditions (i.e., maximum noble gas number densities: $N_{He}\sim 10^{17}$ cm^{-3}, $N_{Ar}\sim 10^{18}$ cm^{-3}) the rates for the endothermic inter-multiplet reactions (Y_{i5}, Y_{i6}, $i=3$, 4) can be neglected in comparison with the total radiative rates ($1/\tau_3$) and ($1/\tau_4$) (see Table 2), because they are almost three orders of magnitude smaller. It is assumed here that the rates Y_{i5} and Y_{i6} are entirely due to collisions with noble gas perturbers. Strictly speaking, they also include the contribution due to collisions with cesium ground state atoms. The cross-section for this particular inter-multiplet mixing induced by cesium has not yet been reported. However, even if we overestimate conservatively this cross-section and take it to be as large as for the intra-multiplet processes (see Table 1), the corresponding rate at the present cesium ground state densities (maximum: 1×10^{13} cm^{-3}) would be one order of magnitude smaller than the noble gas-induced mixing rate. As a consequence, it can also be neglected in the evaluation of the results. In addition, the inter-multiplet mixing rates Y_{53} and Y_{54} are negligible in comparison with the total radiative rate ($1/\tau_5$). Therefore, when all these considerations are taken into account, the first three equations of the above system (3) can be written in the following simplified form:

$$-(1/\tau_3+X_{34})N_3+X_{43}N_4+(A_{53}+Y_{53})N_5+Y_{63}N_6=0 \tag{4}$$

$$X_{34}N_3-(1/\tau_4+X_{43})N_4+(A_{54}+Y_{54})N_5+(Y_{64}+A_{64})N_6=0 \tag{5}$$

$$-(1/\tau_5+X_{56})N_5+X_{65}N_6=0 \tag{6}$$

From Eqs. (4) and (5), using the experimentally obtained population ratios N_3/N_6, N_4/N_6 and N_5/N_6 and the cross-section data Q_{34} and Q_{43} given in Table 1, the following quantities can be determined:

$$Y_{63}+Y_{53}\frac{N_5}{N_6}=(1/\tau_3+Q_{34}v_{Cs-P}N_P)\frac{N_3}{N_6}-Q_{43}v_{Cs-P}N_P\frac{N_4}{N_6}-A_{53}\frac{N_5}{N_6} \tag{7}$$

$$Y_{64}+Y_{54}\frac{N_5}{N_6}=(1/\tau_4+Q_{43}v_{Cs-P}N_P)\frac{N_4}{N_6}-Q_{34}v_{Cs-P}N_P\frac{N_3}{N_6}-A_{64}-A_{54}\frac{N_5}{N_6}. \tag{8}$$

In the above equations, v_{Cs-P} is the mean Maxwellian velocity of the colliding cesium–perturber pair (P=He, Ar) and N_P is the perturber number density.

In the present experiment, we were not able to selectively determine the rates Y_{6i} and Y_{5i} ($i=3$, 4). From the mathematical point of view, it is possible to plot the experimentally determined quantities $Y_{6i}+Y_{5i}$ (N_5/N_6) as a function of (N_5/N_6) and obtain Y_{6i} and Y_{5i} from the intercepts and the slopes of the corresponding straight lines.

Table 1
Existing literature data for the cross-sections of collisional excitation energy transfer in the processes Cs(m)+P→Cs(n)+P, where m, n=6D$_J$ or 7P$_J$, and P=Cs, He or Ar

Number	Transition	$m \rightarrow n$	P	$Q^{P}_{mn}(10^{-16}$ cm^2)	T(K)	Reference
Intramultiplet transitions						
1	$7P_{3/2} \rightarrow 7P_{1/2}$	4→3	Cs	107±22	443	[17]
			He	15.1±3	405	[18]
				15.6±3	630	[18]
				11±2	450	[11]
				11±2	615	[11]
			Ar	0.08±0.015	405	[18]
				0.24±0.05	630	[18]
				0.1±0.02	450	[11]
				0.17±0.03	615	[11]
2	$7P_{1/2} \rightarrow 7P_{3/2}$	3→4	Cs	121±25	443	[17]
			He	14.2±3	405	[18]
				20.8±4	630	[18]
				12±2	450	[11]
				13±2	615	[11]
			Ar	0.075±0.015	405	[18]
				0.18±0.04	630	[18]
				0.12±0.02	450	[11]
				0.21±0.04	615	[11]
3	$6D_{5/2} \rightarrow 6D_{3/2}$	6→5	Cs	210±40	483±70	[19]
4	$6D_{3/2} \rightarrow 6D_{5/2}$	5→6	Cs	270±50	483±70	[19]
Intermultiplet transitions						
1	$7P_{1/2} \rightarrow 6D_{3/2}$	3→5	He	0.25±0.08	450	[11]
				0.8±0.2	615	[11]
			Ar	$\leq 2\times10^{-3}$	450	[11]
2	$6D_{3/2} \rightarrow 7P_{1/2}$	5→3	He	1.7±0.5	450	[11]
				2.7±0.7	615	[11]
			Ar	$\leq 1.4\times10^{-2}$	450	[11]
3	$7P_{3/2} \rightarrow 6D_{3/2}$	4→5	He	0.27±0.08	450	[11]
				0.8±0.2	615	[11]
			Ar	$(3.7\pm1.2)\times10^{-3}$	450	[11]
4	$6D_{3/2} \rightarrow 7P_{3/2}$	5→4	He	2.1±0.6	450	[11]
				3.6±1.0	615	[11]
			Ar	$(2.9\pm0.9)\times10^{-2}$	450	[11]

Table 2
Spontaneous emission rates, A, and $1/\tau$ (in units 10^7 s^{-1}) data relevant for the evaluation of the results

No.	Rate	This work	Reference [11]
1	$1/\tau_6$	1.66[a]	
2	$1/\tau_5$	1.66[a]	1.25[b]
3	$1/\tau_4$	0.73[a]	0.82[b]
4	$1/\tau_3$	0.61[a]	0.64[b]
5	A_{64}	0.0064[c]	
6	A_{54}	0.0009[c]	
7	A_{53}	0.0074[c]	
8	A_{62}	1.65[a]	
9	A_{52}	0.283[a]	0.267[b]
10	A_{51}	1.36[a]	0.986[b]
11	A_{30}	0.079[a]	0.158[b]
12	A_{40}	0.177[a]	0.418[b]

The labels of the various rates are explained in the text and in Fig. 2. We report the values used in the present work and those used by other authors to obtain the results that are compared with ours.
[a] Results from Ref. [20].
[b] Values from Ref. [22].
[c] Values calculated using the oscillator strengths published in Ref. [21].

However, it turned out that the Y_{6i} and Y_{5i} determined in this way have error bars too large to be acceptable. Nevertheless, the applied procedure showed that Y_{6i} and Y_{5i} are comparable in value and justified the assumption:

$$Y_{63} \approx Y_{53} \equiv Y_{D3} \tag{9}$$

$$Y_{64} \approx Y_{54} \equiv Y_{D4}. \tag{10}$$

Such assumption was then used in the subsequent analysis. The assumption can be additionally corroborated by considering the difference between the energy defects ΔE for the reactions 6→3 (ΔE_{63}=685 cm^{-1}) and 5→3 (ΔE_{53}=642 cm^{-1}), or 6→4 (ΔE_{64}=866 cm^{-1}) and 5→4 (ΔE_{54}=823 cm^{-1}). The difference between ΔE_{63} and ΔE_{53}, or between ΔE_{64} and ΔE_{54}, amounts to only 43 cm^{-1} which is small in comparison with the value of the particular energy defect. Therefore, based on the general behavior of the exothermic CEET cross-sections with respect to the reaction energy defect (see Ref. [1,3,4]) it can be expected that the

cross-sections for the processes 6→3 and 5→3 (or 6→4 and 5→4) do not differ much.

From Eqs. (7)–(10), the following relations can be derived:

$$Y_{D3} = \frac{(1/\tau_3 + Q_{34} v_{Cs-P} N_P)(N_3/N_6) - Q_{43} v_{Cs-P} N_P N_4/N_6 - A_{53} N_5/N_6}{1 + (N_5/N_6)} \tag{11}$$

$$Y_{D4} = \frac{(1/\tau_4 + Q_{43} v_{Cs-P} N_P)(N_4/N_6) - Q_{34} v_{Cs-P} N_P N_3/N_6 - A_{64} - A_{54} N_5/N_6}{1 + (N_5/N_6)}. \tag{12}$$

In analogy with the gas kinetics the rates are usually defined as $Y_{Di} = Q_{Di} v_{Cs-P} N_P$ (i=3,4). Once the temperature of the vapor, and consequently the mean velocity, are known, the cross-sections Q_{Di} for the collisional excitation transfer processes Cs(6D)+P→Cs(7P$_J$)+P can therefore be obtained from the slope of the straight line Y_{Di} versus N_P.

Additionally, Eq. (6) can be combined with the principle of the detailed balancing:

$$\frac{X_{56}}{X_{65}} = \beta = \frac{g_6}{g_5} \exp\left(-\frac{\Delta E_{65}}{kT}\right) \tag{13}$$

resulting in the following relation for the intramultiplet mixing rate:

$$X_{65} = \frac{1}{\tau_5 N_6} \frac{N_5}{1 - \beta N_5/N_6} \tag{14}$$

for the process Cs(6D$_{5/2}$)+P→Cs(6D$_{3/2}$)+P (P=He, Ar). In Eq. (13) g_5 and g_6 are the statistical weights of the levels 5 and 6, respectively. Again, the corresponding cross-sections Q_{65}^{P} are obtained from the slope of the straight line X_{65} versus N_P. The numerical values of the rates $1/\tau_i$ and A_{ij} used to evaluate relations (11), (12) and (14) are given in Table 2.

2.3. Determination of the relevant population ratios, the cesium ground-state number density and the vapor temperature

The transitions involved in the determination of the relative number densities in the excited cesium states are indicated in the cesium partial term diagram shown in Fig. 2.

The evaluation of the cross-sections for the processes (1) and (2) required the determination of the population ratios N_3/N_6, N_4/N_6 and N_5/N_6 (see Fig. 2 for labels) as a function of noble gas (He, Ar) pressure. These population ratios were determined by the measurement of the relevant relative fluorescence intensities.

The fluorescence zone had the cylindrical shape (radius $r \approx 0.1$ cm) defined by the laser beams. At present experimental conditions the optical depths $k_0 r$ (k_0 is the peak absorption coefficient) on the path across the excitation zone were much smaller than unity for all relevant lines (917, 921, 455 and 459 nm). Therefore, the lines corresponding to the 7P$_{3/2}$→6S$_{1/2}$(4→0), 7P$_{1/2}$→6S$_{1/2}$(3→0), 6D$_{5/2}$→6P$_{3/2}$(6→2) and 6D$_{3/2}$→6P$_{3/2}$(5→2) transitions, emerging from the excitation volume were optically thin. By applying the analysis of radiation trapping effects developed for the infinite cylinder [3], which suits the present excitation geometry, the radiation trapping within the excitation volume for all considered lines was found to be negligible.

The fluorescence intensity of the optically thin line, observed with a monochromator having the band-pass (0.8 and 0.1 nm for M1 and M2, respectively) large in comparison with the width of the line, is spectrally integrated over the frequencies within the whole line profile. Therefore, the total fluorescence intensities I of the lines emerging from the observation volume can be expressed as:

$$I_{ij} \propto h v_{ij} \cdot A_{ij} \cdot N_i \tag{15}$$

where A_{ij} denotes the spontaneous emission coefficient for the $i \rightarrow j$ transition, N_i labels the population of the emitting level, and v_{ij} is the frequency of the transition. Therefore, the population ratios needed for the cross-section evaluation are given by:

$$\frac{N_3}{N_6} = \frac{v_{62}}{v_{30}} \frac{A_{62}}{A_{30}} \frac{I_{30}}{I_{62}} \tag{16}$$

$$\frac{N_4}{N_6} = \frac{v_{62}}{v_{40}} \frac{A_{62}}{A_{40}} \frac{I_{40}}{I_{62}} \tag{17}$$

$$\frac{N_5}{N_6} = \frac{v_{62}}{v_{52}} \frac{A_{62}}{A_{52}} \frac{I_{52}}{I_{62}}. \tag{18}$$

The numerical values of the spontaneous emission rates A_{ij} used in the evaluation are given in Table 2.

At the ground state cesium densities of the present experiment, the blue fluorescence lines at 455 and 459 nm were slightly optically thick at the path $\tilde{L} = L/2$ from the excitation zone to the exit window. Therefore the measured blue fluorescence signals I_{40} and I_{30} were corrected for the corresponding absorption. The details about the correction procedure are given in [12]. All the intensities reported in Eqs. (16)–(18) were corrected for the spectral response of the Jarrell–Ash detection system as explained in Section 2.1.

The cesium ground state density N_{Cs} was needed for the evaluation of the absorption correction factors for the blue fluorescence intensities and the determination of the vapor temperature. The N_{Cs} values in the investigated temperature range were obtained using the absorption coefficients measured at the outer wings of the hyperfine components of the cesium D2 line. Details of the N_{Cs} determination can be found in [12,23]. The numerical values of the physical constants needed were the oscillator strengths of the hyperfine components of the Cs D2 line ($f_{weak}=0.310$ and $f_{strong}=0.398$ [3]), the natural lifetime of the Cs($6P_{3/2}$) state ($\Gamma_N=5.18$ MHz [20]), and the broadening parameters for the Cs-noble gas interaction ($\gamma_{Cs-He}=(3.6\pm0.5)\times10^{-10}$ s^{-1} cm^3, $\gamma_{Cs-Ar}=(3.4\pm0.5)\times10^{-10}$ s^{-1} cm^3 [24]), and the Cs–Cs interaction ($\gamma_{Cs-Cs}=(6.7\pm1)\times10^{-7}$ s^{-1} cm^3 [25]).

The cesium ground-state number densities N_{Cs} in the investigated temperature range were found to be between 1×10^{12} cm^{-3} and 1×10^{13} cm^{-3}, and the corresponding temperatures, obtained from the vapor pressure curve, were in the range between 333 an 367 K.

The determination of N_{Cs} was affected by a statistical error of ±20%. The contributions to the uncertainty of N_{Cs} come from the error in the determination of the absorption coefficient (±17%) and the uncertainty of the broadening parameters γ_{Cs-He} and γ_{Cs-Ar} taken from literature (the latter introduce errors of ±1% and ±12%, respectively).

The temperature of the vapor was used to obtain the Maxwellian mean relative velocity $v=(8k_BT/\pi\mu)^{1/2}$ of the colliding cesium and noble gas atoms (k_B is the Boltzmann constant and μ is the reduced mass of Cs-noble gas quasimolecule), which was needed for the determination of the cross-sections. Since the temperature was read off the N_{Cs} vs. T curve [13,14], the error in T was as much as the error of ±20% in the N_{Cs} produced, i.e., ±3 K. Consequently, the uncertainty in the relative velocity would be less than ±1%. Allowing also for the possible uncertainty in the vapor pressure curve we have estimated the error in v to be at most ±3% (at the experimental temperature $T\sim350$ K an uncertainty of ±20 K accounts for the stated error).

3. Results and discussion

Fluorescence intensities I_{40} (455 nm), I_{30} (459 nm), I_{62} (917 nm) and I_{52} (921 nm) were measured at various noble gas pressures and at three cesium ground-state densities, in the way described in Section 2. In the case of helium, the measurements were carried out at $N_{Cs}=1\times10^{12}$, 3×10^{12}, 5×10^{12} cm^{-3} ($T=333$, 350, 356 K) and the He pressure was varied in the range between 0.25–12.2 mbar. Measurements in argon were done at ground state cesium densities $N_{cs}=2\times10^{12}$, 5×10^{12}, 1×10^{13} cm^{-3} ($T=343$, 356, 367 K), while the Ar pressure was changed from 5 to 114 mbar.

From the general features of the fluorescence radiation, it follows that the relaxation of the collisionally populated states will result in an isotropic an unpolarized emission, while the resonance fluorescence due to the optical excitation by a linearly polarized laser is expected to be polarized and anisotropic. In the present case, all but 917 nm fluorescence intensities used in the evaluation originate from the collisionally populated levels and are spatially isotropic. Since the resonance fluorescence signal (917 nm line, $J=5/2\rightarrow J=3/2$ transition) is expected to exhibit polarization anisotropy, it was checked against polarization effects. They were found to be negligible for noble gas pressures higher than 2 mbar, and were therefore neglected in the evaluation of the cross-sections.

The fluorescence signals were also checked against laser-scattered light. The background due to 852 nm scattered light was not detectable in any of the measured signals. The background due to 917 nm laser was present only in the resonance fluorescence signals (between 2% and 5% of the total 917 nm signals) and it was subtracted form the measured 917 nm intensities.

The population ratios N_3/N_6, N_5/N_6 and N_4/N_6 needed for the evaluation of the cross-sections were determined from the measured fluorescence intensities using Eqs. (16)–(18). Figs. 3 and 4 show the results obtained as a function of the perturber number density (He and Ar, respectively). In both figures, for visual clarity, instead of plotting N_3/N_6 (which is difficult to distinguish from N_4/N_6), the ratio N_3/N_4 is shown. The latter is calculated using relation analogous to (16)–(18). Moreover, the ratio $N_3/N_6=(N_3/N_4)\times(N_4/N_6)$ for each perturber can be obtained from the data plotted in Figs. 3 and 4. The data were obtained at three different cesium ground state densities, and the fluorescence intensities used for the evaluation of N_3/N_4 were corrected for the absorption along the exit path, as explained in Section 2.3. The good agreement among the data N_4/N_6 and N_3/N_4 obtained at three different cesium ground state densities confirms the validity of the procedure used for correcting the blue fluorescence intensities for absorption.

As can be seen in Figs. 3a and 4a, the ratio N_3/N_4 reaches the thermodynamic equilibrium at He pressure of about 10 mbar, but it is far from the equilibrium value even at 100 mbar of Ar. Such behavior is expected considering the cross-sections for the He and Ar-induced $7P_J$ fine structure mixing. Namely, at the temperatures in the present experiment the cross-section for this process induced by He is more than two orders of magnitude larger than for Ar as a perturber (see Table 4). Therefore in Ar case the ratio N_3/N_4 should reach the thermodynamic equilibrium at correspondingly larger pressures (at least one order of magnitude higher than the highest Ar pressure applied in the present experiment).

In the case of He as a perturber both N_5/N_6 and N_3/N_4 reach the equilibrium at similar pressures (Fig. 3a). This indicates that the cross-sections for the $7P_J$ and $6D_J$ fine structure mixing are of the same order of magnitude. On the other hand the results for N_5/N_6 and N_3/N_4 displayed in Fig. 4a for the case of collisions with Ar, suggest that the

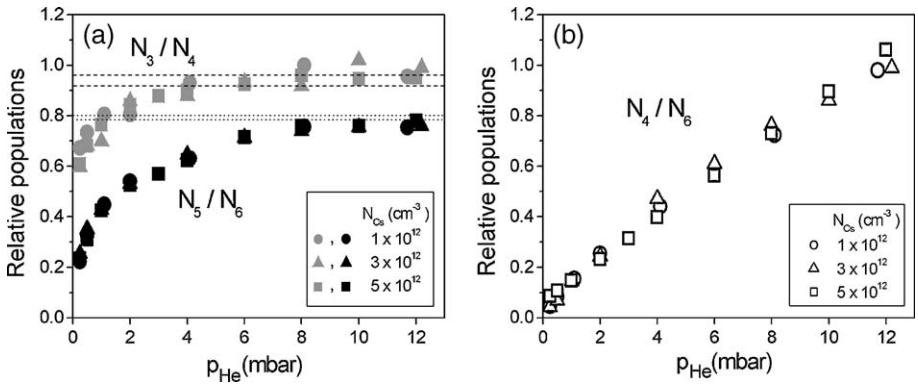

Fig. 3. Behavior of the population ratios N_3/N_4, N_5/N_6 and N_4/N_6 as a function of He number density, determined using the measured fluorescence intensities (see Section 2.3). The indices correspond to the level labeling reported in Fig. 2. The data were obtained at three different cesium ground state densities, and the fluorescence intensities used for the evaluation of N_3/N_4 were corrected for absorption, as explained in Section 2.3. The dashed and dotted lines in part (a) of the figure indicate the thermodynamic equilibrium ratios for N_3/N_4 and N_5/N_6, respectively, at the minimum (333 K) and maximum (356 K) temperatures investigated.

cross-section for Ar-induced $6D_J$ mixing is much larger than the one for $7P_J$ mixing. In the following analysis, both expectations will be confirmed (compare Q_{34}^{He} and Q_{34}^{Ar} given in Table 4 and the present results for Q_{65}^{He} and Q_{65}^{Ar}).

Using the population ratio data displayed in Figs. 3 and 4, the collisional transfer rates Y_{D3} and Y_{D4} for the processes $Cs(6D_{3/2,\ 5/2})+P \rightarrow Cs(7P_{1/2})+P$ and $Cs(6D_{3/2,\ 5/2})+P \rightarrow Cs(7P_{3/2})+P$ induced by helium and argon were calculated according to Eqs. (11) and (12). The results plotted against the perturber number density are shown in Figs. 5 and 6 for helium and argon, respectively. The straight lines displayed in figures represent the least square fits through the experimental data.

From the slopes of the straight lines the following values for the corresponding cross-sections were calculated: $Q_{D3}^{He}=(0.9\pm0.4)\times10^{-16}$ cm^2, $Q_{D4}^{He}=(2.6\pm1.2)\times10^{-16}$ cm^2, $Q_{D3}^{Ar}=(1.2\pm0.6)\times10^{-18}$ cm^2, $Q_{D4}^{Ar}=(2.6\pm1.3)\times10^{-18}$ cm^2. The results are summarized in Table 3. In the evaluation of the cross-sections the average temperature corresponding to the covered temperature range was used to obtain the mean Maxwellian velocity of the colliding atom pairs. The cross-sections for He and Ar perturbers were determined with the accuracy of ±45% and ±50%, respectively. The errors include the contributions from the uncertainties of the fluorescence intensities I_{52}, I_{62}(5% to 15%) and I_{30}, I_{40} (15% to 30%), the error in the determination of the absorption correction factors for the blue fluorescence signals (from 7% to 20% as noble gas pressure decreased), the uncertainty of the relative velocity (3%) of the Cs-noble gas collision pairs, and statistical error (±15%) of the straight line fit through Y versus N_P data. Additionally, at noble gas pressures <2 mbar, the resonance fluorescence intensity I_{62} was plagued with systematic error due to polarization effects, which were not taken into account (an estimate based on the test made with the polarization analyzer gave an uncertainty of 20%). Finally, the error introduced by the uncertainty of the noble gas density was negligible.

In the literature, only one investigation dealing with the evaluation of the cross-section for the He and Ar-induced collisional $7P \rightarrow 6D$ excitation transfer in cesium has been previously reported by Cuvellier et al. [11]. The authors have evaluated J-selective cross-sections for the endothermic processes $Cs(7P_{1/2}) \rightarrow Cs(6D_{3/2})$ and $Cs(7P_{3/2}) \rightarrow Cs(6D_{3/2})$ (Q_{35} and Q_{45} in the present notation) at temperatures of 450 and 615 K. To enable a comparison of the present results with the values published in [11], the principle of the detailed

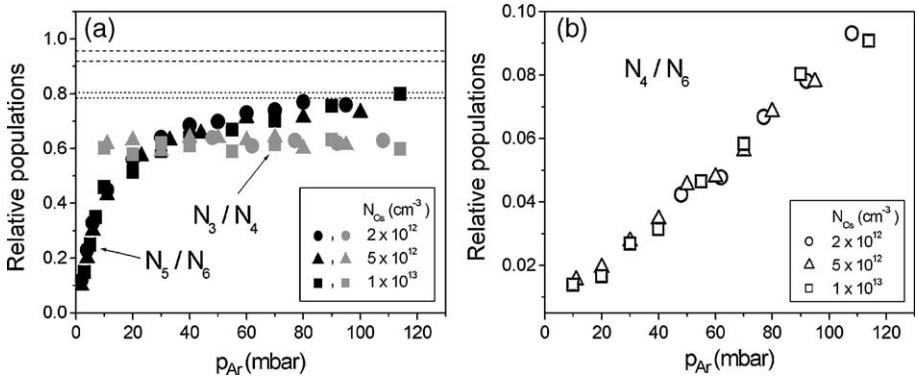

Fig. 4. Same as for Fig. 3, with argon as perturber.

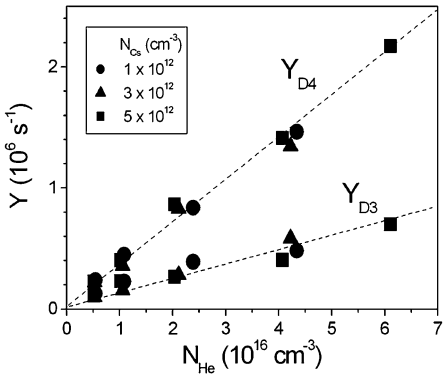

Fig. 5. Collisional transfer rates (Y_{D3} and Y_{D4}) for the processes Cs $(6D_{3/2,\ 5/2})$+He→Cs$(7P_{1/2})$+ He and Cs$(6D_{3/2,\ 5/2})$+He→Cs$(7P_{3/2})$+ He, resectively, as functions of helium number density.

balancing was applied to these data in order to obtain the cross-sections Q_{53} and Q_{54} for the corresponding exothermic reactions. The resulting values are listed in Table 3. In the end, the numerical values of the cross-sections determined experimentally will depend on the choice of the spontaneous emission rates and radiative lifetimes of the involved states entering the evaluation of the relevant population ratios and the corresponding steady state rate equations. In their calculations, Cuvellier et al. [11] used Warner's [22] A-values listed in Table 2. In the present investigation, more recent A- and $(1/\tau)$-values, taken from [20], were used. To put the results on a common ground for comparison, the cross-sections of Cuvellier et al. [11] have been recalculated using our set of A and $(1/\tau)$ values. These recalculated values (herewith denominated Q_{53}^{r} and Q_{54}^{r}) are also given in Table 3. It can be seen that the values $Q_{D3}\equiv Q_{53}\approx Q_{63}$ and $Q_{D4}\equiv Q_{54}\approx Q_{64}$ determined here agree with Q_{53}^{r} and Q_{54}^{r} within their estimated uncertainties.

An empirical relationship between the magnitude of the exothermic CEET cross-sections and their dependence on temperature, based on the collection of data available in literature, has recently been published [3]. The cross-sections for Cs$(6D_{3/2})$→Cs$(7D_J)$ transfer induced by helium measured presently at $T=350\pm20$ K, together with the data of [11] obtained at 450 and 615 K, allow to estimate the temperature trend of these cross-sections. When added

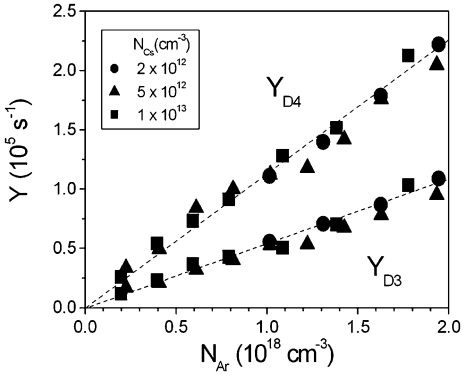

Fig. 6. Same as Fig. 5, with argon as perturber.

Table 3
Cross-sections Q_{53} and Q_{54} for the collisional transfer Cs$(6D_{3/2})$→Cs$(7P_{1/2})$ and Cs$(6D_{3/2})$→Cs$(7P_{3/2})$, respectively, induced by He and Ar

Perturber	Q (10^{-16} cm^2)	$T=350\pm20$ K	$T=450$ K	$T=615$ K
He	$Q_{D3}\equiv Q_{53}\approx Q_{63}$	*0.9±0.4*	–	–
	$Q_{D4}\equiv Q_{54}\approx Q_{64}$	*2.6±1.2*	–	–
	Q_{53}^{r}	–	1.1±0.3	1.8±0.5
	Q_{54}^{r}	–	1.2±0.3	2.1±0.6
	Q_{53}	–	1.7±0.5	2.7±0.7
	Q_{54}	–	2.1±0.6	3.6±1.0
Ar	$Q_{D3}\equiv Q_{53}\approx Q_{63}$	*0.012±0.006*	–	–
	$Q_{D4}\equiv Q_{54}\approx Q_{64}$	*0.026±0.013*	–	–
	Q_{53}^{r}	–	~0.009	–
	Q_{54}^{r}	–	0.015±0.005	–
	Q_{53}	–	~0.014	–
	Q_{54}	–	0.029±0.009	–

The reported values of Q_{53} and Q_{54} are the results of Cuvellier et al. [11], obtained by applying the principle of the detailed balancing to the published data measured for the endothermic reaction. Q_{53}^{r} and Q_{54}^{r} are the results of [11] recalculated using the same spontaneous emission rates and radiative lifetimes of the relevant states as in the present work (see Table 2). The reported values of Q_{D3} and Q_{D4} (in italic letters) are the results of this work.

to field of the Q vs. T curves, these results exhibit the expected behavior (weak increase with increasing temperature) and fit very well into the general scheme for the temperature dependence of the cross-sections for the exothermic CEET processes.

In the case of argon as a perturber, the data points are available only at two temperatures (450 K [11] and 350 K in the present work), their absolute values are very small (~10^{-18} cm^2) and the error bars are relatively large. Such a scanty set of data is insufficient for making conclusive statements about the temperature dependence of the cross-sections for this argon-induced process, or to judge how these data fit into the field of Q vs. T curves for exothermic CEET processes.

The results of the measurements of the intramultiplet mixing rates X_{65} for the process Cs$(6D_{5/2})$+P→Cs $(6D_{3/2})$+P (P=He, Ar) as a function of the perturber number density are displayed in Fig. 7. The rates were

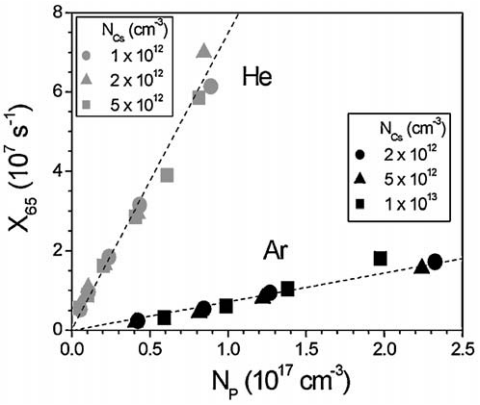

Fig. 7. Collisional mixing rates X_{65} for the processes Cs$(6D_{5/2})$+P→ Cs$(6D_{3/2})$+P (P=He, Ar) as a function of perturber number density.

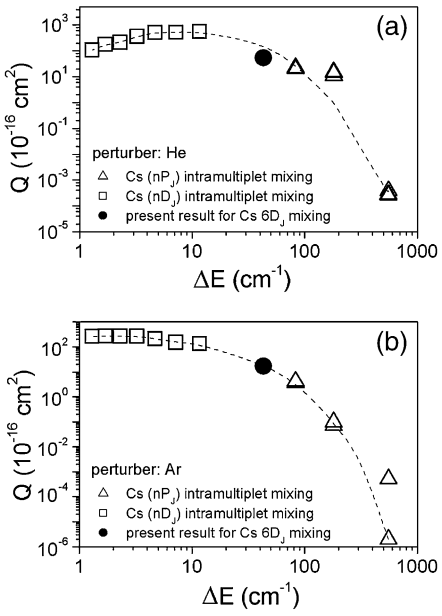

Fig. 8. Cross-sections for intramultiplet ($nP_{1/2}\rightarrow nP_{3/2}$, $nD_{5/2}\rightarrow nD_{3/2}$) mixing in cesium induced by collisions with helium and argon, plotted in double logarithmic scale versus the reaction energy defect ΔE. The displayed data are listed in Table 4. The dashed line is intended merely as a guide for the eye.

evaluated according to Eq. (14) using the experimentally determined population ratios N_5/N_6 (Eq. (18)) shown in Figs. 3 and 4. Since $X_{65}=Q_{65}v_{Cs-P}N_P$, the slopes of the straight lines shown in Fig. 7 yield the cross-sections for the processes investigated. From the least-square fit through the experimental points, the values were found to be $Q_{65}^{He}=(54\pm15)\times10^{-16}$ cm^2 and $Q_{65}^{Ar}=(17\pm5)\times10^{-16}$ cm^2. The overall accuracy of these cross-sections is ±30%. The contributions to the error bar are due to uncertainties in the determination of the following quantities: the intensities of the infrared 917 and 921 nm lines (5–15%), the relative velocity of the colliding species (±3%), and the statistical error (±15%) associated with the straight line fit through X_{65} versus N_P data. Finally, a systematic error in I_{62} (917 nm) due to polarization effects at pressures <2 mbar (estimated to ±20% by checking I_{62} with a polarization analyzer) that was not taken into account, needs also to be considered.

The cross-sections for the fine structure mixing $Cs(6D_{5/2})\rightarrow Cs(6D_{3/2})$ due to collisions with He or Ar have not yet been reported in literature. As a consequence, the results reported here can only be discussed in the context of how well they fit into the database of cross-sections for various intra-multiplet ($nP_{1/2}\rightarrow nP_{3/2}$, $nD_{5/2}\rightarrow nD_{3/2}$) mixing processes in cesium induced by collisions with helium and argon. This fit is shown in Fig. 8 where the cross-sections are plotted in a double logarithmic scale versus the reaction energy defect ΔE. It can be seen that our present data follow very well the trend indicated by the previous results which are listed in Table 4.

4. Conclusion

In this work, the cross-sections $Q_{D3}^{He}=(0.9\pm0.4)\times10^{-16}$ cm^2, $Q_{D4}^{He}=(2.6\pm1.2)\times10^{-16}$ cm^2, $Q_{D3}^{Ar}=(1.2\pm0.6)\times10^{-18}$ cm^2, $Q_{D4}^{Ar}=(2.6\pm1.3)\times10^{-18}$ cm^2 (where the indices 3 and 4 stand for $7P_{1/2}$ and $7P_{3/2}$, respectively) for the processes $Cs(6D)+He,\ Ar\rightarrow Cs(7P_J)+He$, Ar were determined at (350±20) K, and found to be consistent with the cross-sections for the same process reported at higher temperatures [11]. In addition, the cross-section for the fine-structure mixing of the $6D_J$ states induced by collisions with He and Ar were also measured and found to be $Q_{65}^{He}=(54\pm15)\times10^{-16}$ cm^2 and $Q_{65}^{Ar}=(17\pm5)\times10^{-16}$ cm^2, respectively. To our knowledge, the cross-sections for these processes

Table 4
Cross-sections for intra-multiplet $nP_{1/2}\rightarrow nP_{3/2}$, and $nD_{5/2}\rightarrow nD_{3/2}$ mixing in cesium induced by collisions with helium and argon

No.	Cs(2)+P→Cs(1)+P	ΔE_{21}(cm^{-1})	T(K)	Q_{21}^{He}(10^{-16} cm^2)	Q_{21}^{Ar}(10^{-16} cm^2)	Ref.
1	$Cs(6P_{3/2})\rightarrow Cs(6P_{1/2})$	554	311	$(3.9\pm0.4)\times10^{-4}$	$\{5.2\times10^{-4}\}$	[26]
				$(2.7\pm0.4)\times10^{-4}$	2×10^{-6}	[27]
2	$Cs(7P_{3/2})\rightarrow Cs(7P_{1/2})$	181	405	15±3	0.072±0.02	[28]
			630	15.6±3	0.180±0.04	[28]
			450	11±2	0.10±0.02	[11]
			615	11±2	0.17±0.03	[11]
3	$Cs(8P_{3/2})\rightarrow Cs(8P_{1/2})$	83	420	{22.5±7}	{3.6±1.1}	[29]
			620	{20.6±6}	{4.2±1.3}	[29]
4	$Cs(8D_{5/2})\rightarrow Cs(8D_{3/2})$	11.7	360	{552±83}	{133±21}	[30]
5	$Cs(9D_{5/2})\rightarrow Cs(9D_{3/2})$	7.2	360	{515±77}	{150±27}	[30]
6	$Cs(10D_{5/2})\rightarrow Cs(10D_{3/2})$	4.7	353	{503±100}	{211±42}	[31]
7	$Cs(11D_{5/2})\rightarrow Cs(11D_{3/2})$	3.25	353	{330±66}	{263±54}	[31]
8	$Cs(12D_{5/2})\rightarrow Cs(12D_{3/2})$	2.3	353	{208±54}	{262±67}	[31]
9	$Cs(13D_{5/2})\rightarrow Cs(13D_{5/2})$	1.7	353	{175±54}	{268±80}	[31]
10	$Cs(14D_{5/2})\rightarrow Cs(14D_{3/2})$	1.3	353	{107±33}	{260±80}	[31]

For the processes where the cross-section was originally measured only for the endothermic reaction, the corresponding cross-section for the exothermic process was obtained from the principle of the detailed balancing. These values are given in braces. The various reaction energy defects, ΔE, the experimental temperature and the original references (in square brackets) are also given.

are reported here for the first time. The present results fit very well into the existing body of the cross-section data for intra-multiplet ($nP_{1/2} \rightarrow nP_{3/2}$, $nD_{5/2} \rightarrow nD_{3/2}$) mixing in cesium induced by collisions with helium and argon.

Acknowledgements

This research was supported by NIH Grant 63965-04 and the Ministry of Science, Education and Sport of the Republic of Croatia. T. Correll would like to thank the Institute of Physics in Zagreb for providing her with the opportunity of a working stage and for the kind hospitality.

References

[1] L. Krause, in: J.W. McGowan (Ed.), The Excited State in Chemical Physics, Wiley, NY, 1975, pp. 267–316.
[2] W. Demtröder, Laser Spectroscopy, Springer Verlag, Berlin, 1995.
[3] C. Vadla, V. Horvatic, K. Niemax, Radiative transport and collisional transfer of excitation energy in Cs vapors mixed with Ar or He, Spectrochim. Acta, Part B: Atom. Spectrosc. 58 (2003) 1235–1277.
[4] A. Ekers, M. Glodz, V. Grushevsky, J. Kalvins, J. Szonert, Energy transfer between the ^2S and ^2D states in alkalis: experiments and theory, Can. J. Phys. 79 (2001) 1039–1053.
[5] J.P. Temirov, N.P. Chigarev, O.I. Matveev, N.O. Omenetto, B.W. Smith, J.D. Winefordner, A resonance ionization imaging detector based on cesium atomic vapor, Spectrochim. Acta, Part B: Atom. Spectrosc. 59 (2004) 677–687.
[6] D. Pappas, N.C. Pixley, O.I. Matveev, B.W. Smith, J.D. Winefordner, A cesium resonance fluorescence imaging monochromator, Opt. Commun. 191 (2001) 263–269.
[7] D. Pappas, N.C. Pixley, B.W. Smith, J.D. Winefordn, Diffusion of resonance radiation in atomic vapor imaging, Spectrochim. Acta, Part B: Atom. Spectrosc. 56 (2001) 1761–1767.
[8] N.C. Pixley, T.L. Correll, D. Pappas, O.I. Matveev, B.W. Smith, J.D. Winefordner, Tunable resonance fluorescence monochromator with sub-Doppler spectral resolution, Opt. Lett. 26 (2001) 1946–1948.
[9] N.C. Pixley, T.L. Correll, D. Pappas, B.W. Smith, J.D. Winefordner, Sub-Doppler spectral resolution and improved sensitivity in a cesium resonance fluorescence imaging monochromator, Appl. Spectrosc. 56 (2002) 677–681.
[10] N.C. Pixley, T.L. Correll, D. Pappas, N. Omenetto, B.W. Smith, J.D. Winefordner, Moving object detection using a cesium resonance fluorescence monochromator, Opt. Commun. 219 (2003) 27–31.
[11] J. Cuvellier, P.R. Fournier, F. Gounand, J. Pascale, J. Berlande, Inelastic collisions involving excited cesium atoms at thermal energies, Phys. Rev., A 11 (1975) 846–856.
[12] T.L. Correll, V. Horvatic, N. Omenetto, C. Vadla, J.D. Winefordner, Quantum efficiency improvement of a cesium based resonance fluorescence detector by helium-induced collisional excitation energy transfer, Spectrochim. Acta, Part B: Atom. Spectrosc. 60 (2005) 765–774.
[13] J.B. Taylor, I. Langmuir, Vapor pressure of caesium by the positive ion method, Phys. Rev. 51 (1937) 753–760.
[14] A.N. Nesmeyanov, in: R. Gray (Ed.), Vapor Pressure of the Chemical Elements, Elsevier, Amsterdam, 1963.
[15] C. Vadla, K. Niemax, J. Brust, Energy pooling in cesium vapor, Z. Phys., D At. Mol. Clust. 37 (1996) 241–247.
[16] C. Vadla, Energy pooling in caesium vapour: $Cs^*(6P_J)+Cs^*(6P_J) \rightarrow Cs(6S)+Cs^{**}(6D)$, Eur. Phys. J., D At. Mol. Opt. Phys. 1 (1998) 259–264.
[17] P.W. Pace, J.B. Atkinson, Transfer of electronic excitation between $7^2P_{1/2}$ and $7^2P_{3/2}$ states of cesium induced by collisions with cesium atoms, Can. J. Phys. 52 (1974) 1641–1647.
[18] I.N. Siara, H.S. Kwong, L. Krause, Sensitized fluorescence in vapors of alkali atoms XIV. Temperature dependence of cross sections for $7^2P_{1/2}-7^2P_{3/2}$ mixing in cesium, induced in collisions with noble gas atoms, Can. J. Phys. 52 (1974) 945–949.
[19] A.C. Tam, T. Yabuzaki, S.M. Curry, M. Hou, W. Happer, Inelastic cross sections in $Cs(n\ ^2D_J)+Cs(6\ ^2S_{1/2})$ collisions, Phys. Rev., A 17 (1978) 1862–1868.
[20] W. Hansen, The application of polarisation-influenced Thomas–Fermi ion models to alkali-atom transitions, J. Phys., B At. Mol. Opt. Phys. 17 (1984) 4833–4850.
[21] P.M. Stone, L. Agnew, Plasma broadened cesium lines, Phys. Rev. 127 (1962) 1157–1162.
[22] B. Warner, Atomic oscillator strengths-III. Alkali-like spectra, Mon. Not. R. Astron. Soc. 139 (1968) 115–128.
[23] V. Horvatic, C. Vadla, M. Movre, The collision cross sections for excitation energy transfer in $Rb^*(5P_{3/2})+K(4S_{1/2}) \rightarrow Rb(5S_{1/2})+K^*(4P_J)$ processes, Z. Phys., D At. Mol. Clust. 27 (1993) 123–130.
[24] F. Siegling, K. Niemax, Low-pressure noble gas broadening of the Cs resonance lines, Z. Naturforsch. 39a (1984) 447–454.
[25] Z.J. Jabbour, J. Sagle, R.K. Namiotka, J. Huennekens, Measurement of the self-broadening rate coefficients of the cesium resonance lines, J. Quant. Spectrosc. Radiat. Transfer 54 (1995) 767–778.
[26] M. Czajkowski, D.A. McGillis, L. Krause, Sensitized fluorescence in vapors of alkali metals XIV. Energy transfer in collisions between cesium and inert gas atoms, Can. J. Phys. 44 (1966) 91–103.
[27] A. Gallagher, Rubidium and cesium excitation transfer in nearly adiabatic collisions with inert gases, Phys. Rev. 172 (1968) 88–96.
[28] I.N. Siara, H.S. Kwong, L. Krause, Sensitized fluorescence in vapors of alkali atoms XIV. Temperature dependence of cross sections for $7^2P_{1/2}-7^2P_{3/2}$ mixing in cesium, induced in collisions with noble gas atoms, Can. J. Phys. 52 (1974) 945–949.
[29] M. Pimbert, Transfert d'excitation électronique, par collision atomique, entre niveaux élevés d'un atome de césium, J. Phys. 33 (1972) 331–343.
[30] I. Jackowska, M. Lukaszewski, Cross sections for J mixing in 8D and 9D states of cesium in collisions with noble-gas atoms, J. Phys., B At. Mol. Opt. Phys. 23 (1990) 2097–2104.
[31] M. Lukaszewski, I. Jackowska, J mixing in nD ($n=10-14$) states of cesium induced in collisions with noble-gas atoms, J. Phys. B, Atom., Mol. Opt. Phys. 24 (1991) 2047–2057.